The Effect of using Rigid ISOFIX on the Injury Potential of Toddlers in Near-side Impact Crashes

Tanya Kapoor[1], William Altenhof[1] and Andrew Howard[2]
[1]*University of Windsor, Department of Mechanical, Automotive and Materials Engineering*
[2]*The Hospital for Sick Children, Division of Orthopedic Surgery*

Abstract

This research focuses on the injury potential of children seated in forward facing child safety seats during side impact crashes in a near side seated position. Side impact dynamic sled tests were conducted by NHTSA at Transportation Research Center Inc. using a Hybrid III 3-year-old child dummy in convertible forward/rearward child safety seat. The seat was equipped with a LATCH and a top tether and the dummy was positioned in forward-facing/near-side configuration. The test was completed using an acceleration pulse with a closing speed of 24.1 km/hr, in the presence of a rigid wall and absence of a vehicle body. A fully deformable finite element model of a child restraint seat, for side impact crash investigations, has been developed which has also been previously validated for frontal and far side impacts. A numerical model utilizing a Hybrid III 3-year-old dummy, employing a similar set-up as the experimental sled test was generated and simulated using LS-DYNA®. The numerical model was validated by comparing the head and the chest accelerations, resultant upper and lower neck forces and moments from the experimental and numerical tests. The simulation results were observed to be in good agreement to the experimental observations. Further numerical simulations were completed employing a rigid ISOFIX system with two different cross-sectional geometries for the anchoring mechanism. It was observed from the simulation results that the use of both rigid ISOFIX geometries was effective in reducing resultant chest accelerations by approximately 40 percent. A reduction of approximately 20 to 30 percent was observed in lateral shear and lateral bending of the dummy's neck. Of the two rigid ISOFIX geometries considered, the cross-shaped system effectively reduced the lateral head displacement by 27 percent (6.8 cm).

1. Introduction

According to the National Highway Traffic Safety Administration (NHTSA) and Statistics Canada, motor vehicle crashes are the leading cause of death for children under the age of 14 years in North America [1, 2]. For passenger vehicle child occupants aged birth through 8 years, data from the Fatality Analysis Reporting System (FARS) from 1991–2000 showed that regardless of whether the child was seated in the front seat or rear seat, frontal and side crashes accounted for most child occupant fatalities [3]. Data from NHTSA demonstrated that 22 percent of the 3,018 front seat child fatalities were killed in near side impacts [4]. Of the 3,826 rear seat fatalities, 25 percent involved near side impacts.

Howard et al. [5] found that positioning a child restraint seat (CRS) at the centre of the rear seat was statistically safer than the near-side seat, particularly for restrained child occupants. This conclusion is based on the hypothesis that during vehicle crashes near-side child occupants may have contact with intruding vehicle structures. Newgard et al. [6] found that occupants seated on the near-side or middle-seat of a lateral crash had a higher probability of serious thoraco-abdominal injury compared to far-side occupants, with the probability of thoracic injury being higher than that of abdominal injury at all seat positions.

According to the Motor Vehicle Safety Act, Standard 210.2 [7], the use of a top tether strap is mandatory in conjunction with both lower anchorage and tethers for children (LATCH) and lap seat belt. However, in Europe a rigid International Standards Organizations FIX (ISOFIX)

system is used for anchoring a CRS to the vehicle seat. European ISOFIX [8] is a system for the connection of child restraint systems to vehicles which has two vehicle rigid anchorages, two corresponding rigid attachments on the child restraint system and a mean to limit the pitch rotation of the child restraint system.

Comité de Liaison de la Construction d'Equipements et de Pièces d'Automobiles (CLEPA), and Charlton et al. assessed the comparison between ISOFIX and LATCH in side impact performance utilizing a TNO P3 child dummy [9, 10]. These studies concluded that rigid ISOFIX is superior to LATCH in terms of resultant head and chest accelerations and head injury criteria for side impact crashes. A series of sled tests was performed by Klinich et al. [11] at UMTRI using the Q3s Anthropomorphic Test Device (ATD) and the ECE R44 sled buck to study CRS and paediatric occupant kinematics in far-side impacts in both forward/rearward facing CRS configurations. Rigid ISOFIX retained the head of the dummy within the CRS and eliminated rotation of the CRS for the forward facing CRS configuration.

2. Experimental methods

Sled tests were conducted by NHTSA in 2001 at Test Research Center (TRC). This test, labeled 4585 was a sled test without a vehicle body and in the presence of a side rigid wall [12]. In this test, use of a rigid structure represents the location of a vehicle's side structure, positioned 508 mm (20 inches) from Point Z1 (location of the furthest LATCH anchorage from the rigid wall), adjacent to the child restraint. The structure is essentially rigid, flat surface adjacent to the seat assembly, extending from the seat cushion to a height of approximately 762 mm (30 inches). The structure is extended forward a distance of approximately 813 mm (32 inches), to ensure that head contact would only be with a flat surface. The structure does not yield, and does not significantly bend or flex when loaded, and is covered with an aluminum plate. An acceleration pulse with a closing speed of 24.1 km/h (15 mph) was used in the tests and is illustrated in Figure 1. The test incorporated a Hybrid III 3-year-old child dummy restrained in a forward facing child safety seat, and anchored with LATCH system and a top tether. The dummy was equipped with accelerometers in the head and the chest, and load cells were located in the dummy’s upper and lower neck region. Figure 2 illustrates the test configuration and Figure 3 provides a photograph of the experimental apparatus after testing.

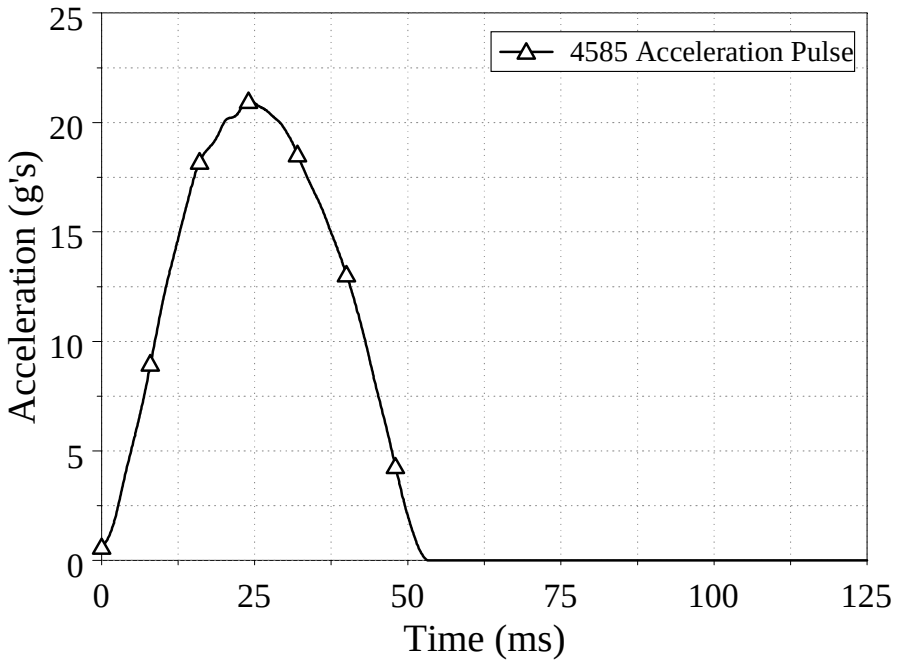

Figure 1. Experimental sled acceleration pulse (Test No. 4585).

Figure 2. Experimental test dummy and CRS configuration.

Figure 3. Qualitative observation from the experimental sled test.

3. Numerical Methods

3.1 CRS modeling

The CRS, as well as all other components of the numerical model including the seat buck, the CRS webbing and the CRS foam pad were meshed using Finite Element Model Builder (FEMB). The child seat was modeled using Computer Aided Design (CAD) surfaces provided by the Century/Graco Corporation. Tensile testing was completed in accordance to ASTM D638M [14] on specimens extracted from various portions of the CRS in order to determine the mechanical characteristics of the CRS polypropylene material under large deformation. The thickness of all thin surfaces of the CRS were measured using a vernier calliper and was observed to be 3.5 mm and 4.5 mm respectively for different panel sections. Two different section properties were generated for the CRS, both incorporating the Belytschko-Tsay shell elements that were assigned a thickness of 3.5 mm and 4.5 mm for both the regions of the CRS. The material model *MAT_PIECEWISE_LINEAR_PLASTICITY was selected to model the material behaviour of the CRS polypropylene. Values for the density, Young's modulus, and Poisson's ratio were 800 kg/m^3, 0.842 GPa and 0.3 respectively. The yield and ultimate tensile strengths of the CRS polypropylene were found to be 8.76 MPa and 18.7 MPa respectively. The mesh of the child seat was comprised of 12,728 nodes and 13,379 shell elements.

3.2 Seatbelt restraints

The seatbelt was modeled to pass through a series of openings and channels of the CRS and to fit around the Hybrid III 3-year-old dummy, which had the same configuration as in all experimental tests. A portion of the seatbelt in the back of the CRS was modeled using one dimensional seatbelt elements, and was connected to the frontal part of the seatbelt which had contact with the child dummy by nodal rigid bodies.

The material model *MAT_FABRIC, was used for the seatbelt webbing. The density, elastic modulus, and Poisson's ratio were specified as 890.6 kg/m^3, 2.068 GPa and 0.3 respectively. Fully integrated Belytschko-Tsay membrane was used for the shell elements of the seatbelt. The material model *MAT_SEATBELT was used to model the one-dimensional seatbelt elements.

*SECTION_SEATBELT was used to define the section properties of the seatbelt elements. The loading/unloading behaviour of the seat belt webbing obtained from material testing is illustrated in Figure 4(a) and was incorporated into the material model for the CRS webbing. Figure 4(b) illustrates the finite element model of the seatbelt, LATCH, top tether, and the five-point restraint system.

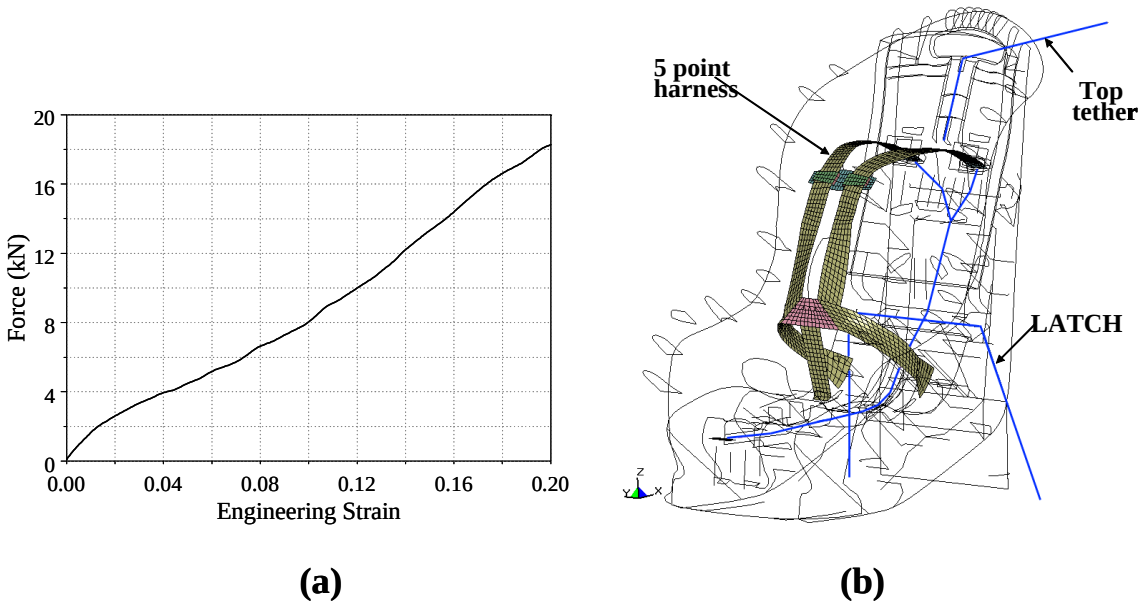

Figure 4. (a) Loading/unloading behaviour of the seatbelt webbing, and (b) the finite element model of the seatbelt, LATCH, top tether, and the five-point restraint system.

3.3 Modeling of the Foam Insert

A foam pad inserted between the polypropylene shell and the seat fabric of the CRS was also incorporated into the FE model of the CRS. The foam was modeled using a selectively reduced solid element formulation. *MAT_LOW_DENSITY_FOAM was selected to model the material behaviour of the solid elements representing the foam pad. This material model was obtained from Turchi et al. [15].

3.4 The Seat Buck

Two parts, namely a rigid seat buck frame and a deformable seat buck pad, were created in order to model the seat buck (vehicle seat bench). The rigid seat buck was modeled using shell elements and the deformable seat buck pad was modeled using solid elements. The identical material model used for modeling the foam pad the CRS was also used for the seat padding. A rigid material definition was selected to model the seat buck frame. The seat buck foam and frame were connected by constraining the outermost nodes of the seat pad to the frame.

3.5 Rigid Wall

A rigid wall was meshed using shell elements on the seat buck which represents the location of a vehicle's side structure, positioned 508 mm from the point Z1, adjacent to the CRS [4]. The rigid wall was meshed extending from the seat cushion to a height of approximately 762 mm. The wall

extended forward a distance of approximately 690 mm, to ensure that head contact would only be with a flat surface.

3.6 Hybrid III 3-year-old dummy

The Hybrid III 3-year-old finite element child dummy model used in this study was developed by First Technology Safety Systems (FTSS). No alterations of the FE model obtained from FTSS were applied and the default values for the materials, joints and element formulations were utilized. Detailed information of the Hybrid III child dummy can be found in reference [16]. The dummy positioning was completed using FEMB.

3.7 Simulation procedure

Tightening of the front-adjusting harness strap was simulated quasi-statically to properly position the child dummy into the CRS. This process was achieved prior to the application of the acceleration pulse to the seat buck through dynamic relaxation. In this stage, the front-adjusting harness strap as well as the upper tether and lower LATCH anchor were preloaded. Loads assigned to the LATCH and the top tether in the dynamic relaxation phase was of a magnitude of 60 N [3] in the direction of the tethers. Contact between the Hybrid III and the CRS, including the webbing, buckles, foam padding and surfaces of the CRS was achieved through a penalty based contact algorithm. The acceleration pulse obtained from the experimental sled test 4585 (Figure 1) was prescribed to the rigid portion of the seat buck. All numerical simulations were conducted using LS-DYNA version 970 5434a [17] on a personal computer equipped with dual 2.6 GHz AMD Athlon processors with 2 gigabytes of RAM. Figure 5 illustrates the isometric view of the complete FE model of the Hybrid III 3-year-old dummy seated in the CRS and the initial configuration of the numerical model in accordance to FMVSS 213 norms.

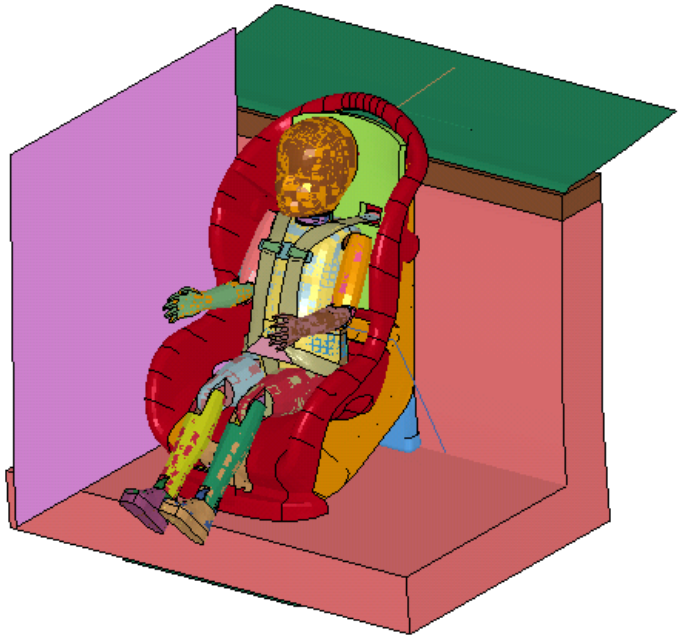

Figure 5. Hybrid III 3-year-old child dummy seated in the CRS for the rigid-wall near-side impact test.

4. Data Analysis

Child occupant injury data was extracted from the instrumentation, including accelerometers and load cells, equipped within the dummy model. All the data was measured with respect to the dummy's local coordinate system as outlined in SAE J211 [13] and was sampled at rate of 10 kHz. The numerical results were filtered in accordance to SAE J211 [13].

The resultant head and chest accelerations were computed using equation 1 where *x*, *y* and *z*-axes are the local coordinate system located at the head and spine locations respectively.

$$a_{\text{resultant}} = \sqrt{a_x^{\,2} + a_y^{\,2} + a_z^{\,2}} \tag{1}$$

The resultant neck forces and moments were computed using equation 2 and equation 3 respectively where the *x*, *y*, and *z*-axes are the local coordinate systems located at each neck location.

$$F_{\text{resultant}} = \sqrt{F_x^{\,2} + F_y^{\,2} + F_z^{\,2}} \tag{2}$$

$$M_{\text{resultant}} = \sqrt{M_x^{\,2} + \mathrm{M}_y^{\,2} + M_z^{\,2}} \tag{3}$$

4.1 Head Injury Criteria

The resultant head acceleration (Equation 1) was used in calculating the Head Injury Criteria (*HIC*) using the Equation 4.

$$HIC_{t_2-t_1} = \left[\frac{1}{t_2 - t_1} \int_{t_1}^{t_2} a_{\text{resultant}} \cdot dt \right]^{2.5} \cdot (t_2 - t_1) \tag{4}$$

5. Model Validation

Finite element model validation was completed by comparing the numerical simulation results with the experimental findings from the side impact tests which involved the Hybrid III dummy only.

5.1 Head acceleration in the local *y*-direction

Figure 6 shows the experimental and numerical results of the child dummy's head accelerations in the local *y*-direction as a function of time. The acceleration response of the Hybrid III dummy from the numerical simulation showed similarities to the experimental results. The minimum values for *y*-axis head acceleration were observed to be -45 g's for the numerical simulations and -51 g's for the experimental dummy respectively. The time to reach the peaks was approximately 60 ms for both the tests.

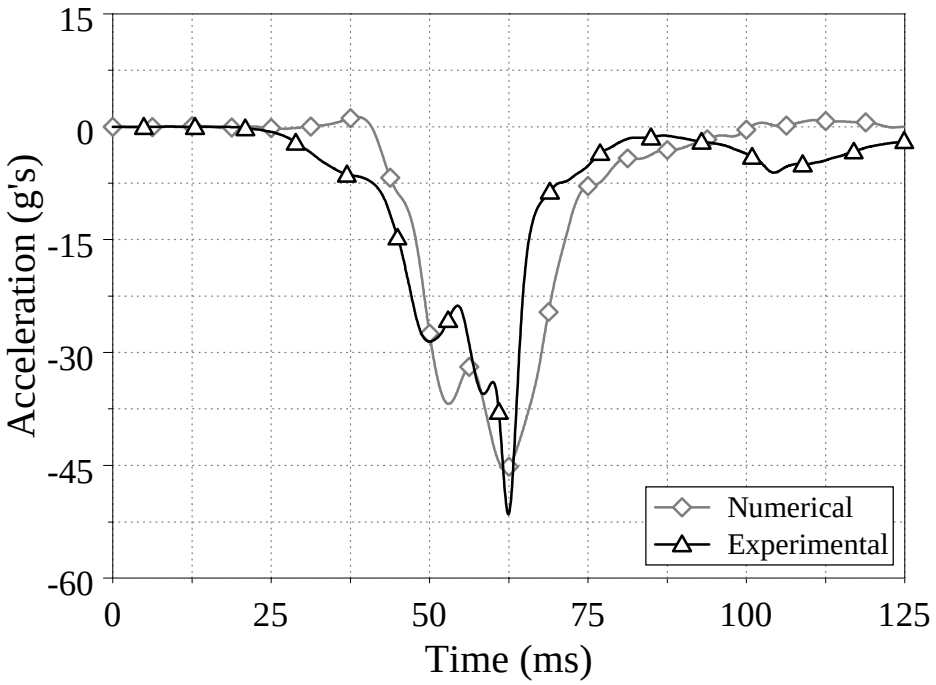

Figure 6. Experimental and numerical head acceleration in local y-axis direction as a function of time.

5.2 Chest acceleration in the local *y*-direction

The chest accelerations in local *y*-direction as a function of time are presented in Figure 7. Similar time profiles were observed for both the experimental and numerical observations. The peak values for the chest acceleration in local *y*-axis direction were observed to be approximately -69 g's for both the numerical and experimental tests. The time to reach the peaks was approximately 50 ms for both the cases.

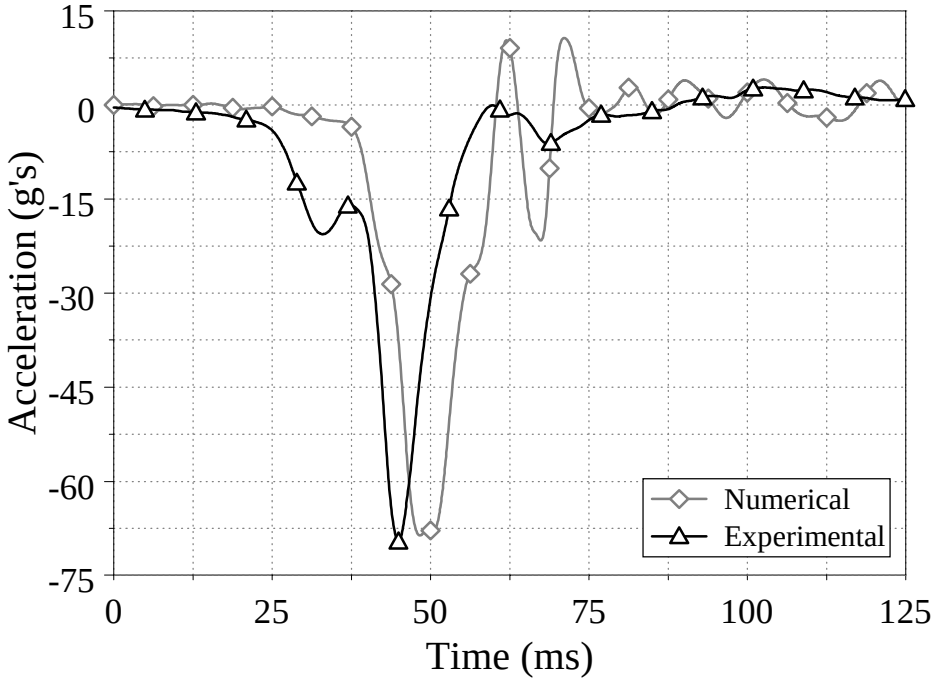

Figure 7. Experimental and numerical chest acceleration in local *y*-axis direction as a function of time.

5.3 Resultant upper and lower neck forces

Figure 8 and Figure 9 respectively demonstrate the resultant upper and lower neck forces experienced by the child dummy. Numerical simulations exhibited similar time profiles for the resultant neck loads with a difference in peak values. The maximum values for the resultant upper neck forces were 965 N and 1177 N for experimental and numerical tests respectively. The maximum values for the resultant lower neck forces were observed to be 1021 N for the experimental child dummy, and 1288 N for the numerical child dummy respectively. The numerical model over predicted the resultant peak neck forces from experimental tests by approximately 20 percent.

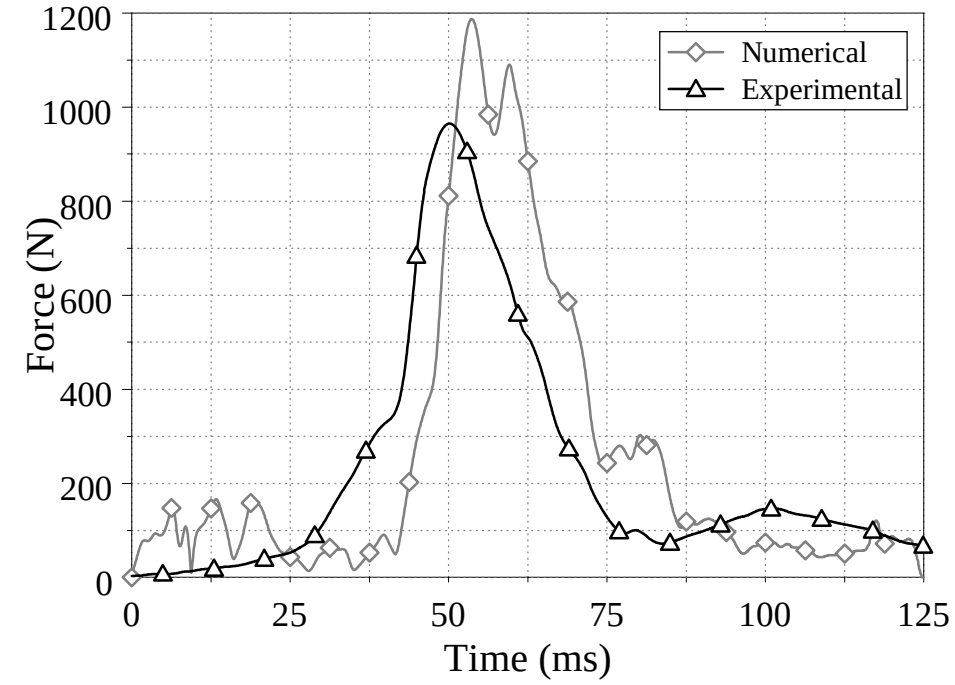

Figure 8. Experimental and numerical resultant upper neck force as a function of time.

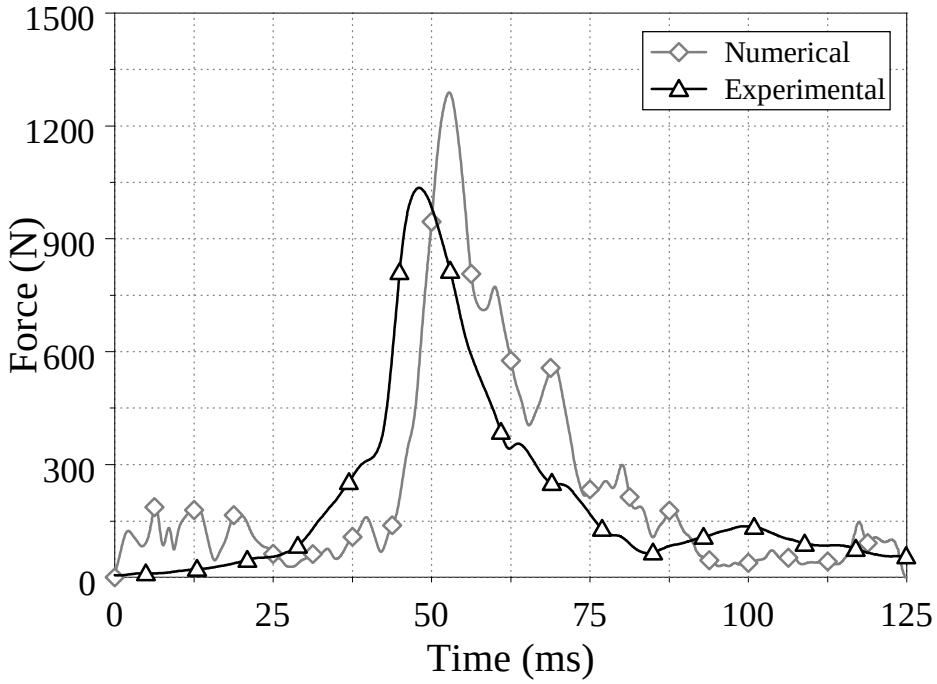

Figure 9. Experimental and numerical resultant lower neck force as a function of time.

5.4 Resultant upper and lower neck moments

The time profiles for the resultant upper and lower neck moments of the child dummy are illustrated in Figure 10 and Figure 11 respectively. The resultant upper and lower neck moments of the child dummy were over predicted by the numerical model. Variation in peak values for resultant upper and lower neck moments may be due to the use of different child restraining systems. The peak resultant upper neck moments were 45 N·m and 75 N·m for experimental and numerical tests respectively. The respective peak resultant lower neck moments were 105 N·m for the experimental child dummy and 165 N·m for the numerical child dummy. It should be noted that the maximum moments were observed at approximately 60 ms for the numerical dummy.

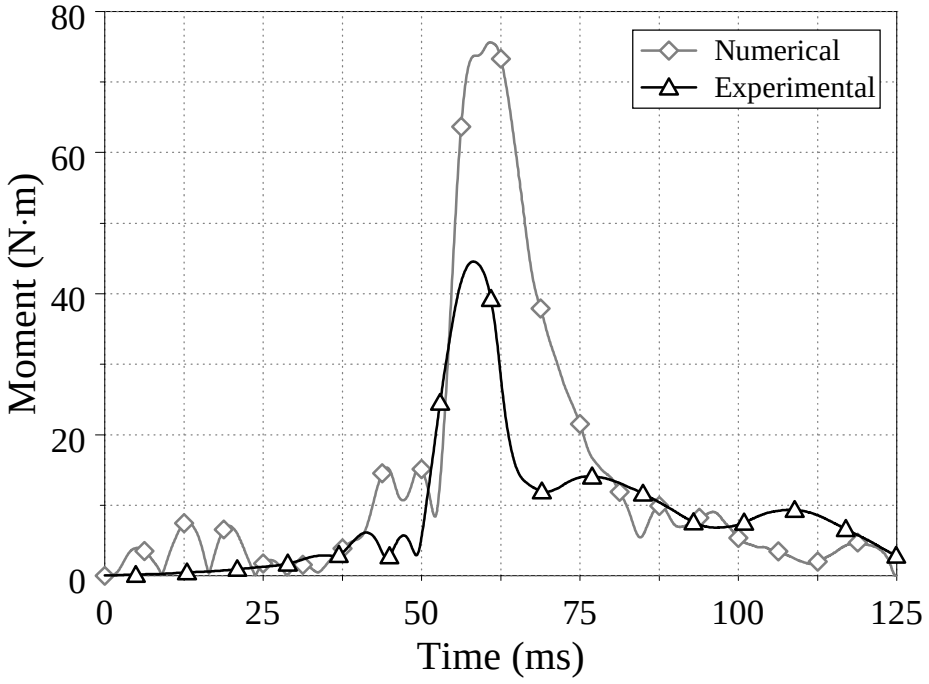

Figure 10. Experimental and numerical resultant upper neck moment as a function of time.

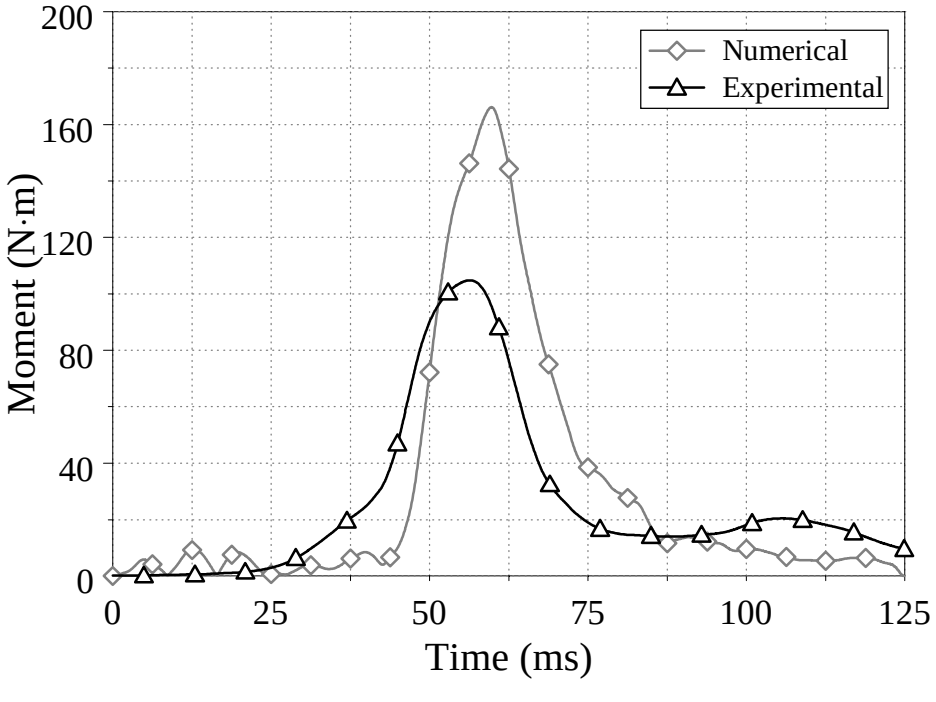

Figure 11. Experimental and numerical resultant lower neck moment as a function of time.

An acceptable agreement between the numerical simulation results and the experimental findings shows the numerical models' ability to predict the kinematic and kinetic response, which the Hybrid III 3-year-old child dummy experienced in near-side impact sled tests. This model has previously been validated for far-side crash conditions [18].

6. Countermeasure Development

There are a considerable number of uncertainties in a vehicle crash and child injury mechanisms for side impacts at the present time, which may inhibit the development of a novel device to significantly reduce the possibility of injury. In this research, the use of rigid ISOFIX system as a means for anchoring the CRS, and energy absorbing foams as methods to attenuate injuries in side impacts have been investigated. In near-side impact situations the main cause of injury is contact related [5, 6]. Therefore a reduction in lateral displacement of the CRS and the child's head can attenuate the amount of injury sustained in near-side crashes.

A rigid ISOFIX system with rectangular cross section, as outlined in United Nations Economic Commission for Europe (UNECE) Regulation 14 [8] was modeled as a method of anchoring CRS to the vehicle seat using FEMB. In addition, a cross shaped ISOFIX system was also investigated. Figure 12 illustrates the three different anchoring methods used in this research. A cross-shaped ISOFIX system would limit the lateral displacement of the CRS more compared to the rectangular shaped ISOFIX system. Both the ISOFIX systems were modeled using fully integrated shell elements and were assigned material properties of steel (Elastic modulus = 207 GPa, density = 7.8 g/cm^3, poisson's ratio = 0.3). An elastic/plastic

behaviour was defined for the ISOFIX systems with the yield strength of 210 MPa and the ultimate tensile strength of 475 MPa. The linear dimensions of the rectangular section ISOFIX system were 67 mm length, by 30 mm height, by 3 mm thickness. The cross-shaped section ISOFIX system comprised of two mutually perpendicular rectangular sections at the center, with same cross section dimensions of the individual rectangular section. The ISOFIX was constrained to the CRS and the vehicle seat using constrained extra nodes card. Simulations were completed utilizing a Hybrid III 3-year-old dummy with all the three anchoring methods under the identical acceleration pulse for side impact.

Wang et al. [18] have investigated the use of energy absorbing foams as a method to attenuate injuries in side impacts. Energy absorbing foam was added in the region of the CRS where contact between the child's head and the CRS may occur during side impacts. It was expected that during side crashes the dummy's head would contact the energy absorbing foam and the corresponding foam deformation would help minimize the lateral displacement of the head and the injury probability. Material characteristics were identical to the padding on the back of the CRS as taken from Turchi et al. [15]. Contact between the energy absorbing foam and the CRS was modeled using a tied nodes to surface contact algorithm. Figure 13 depicts the modified CRS with the additional side foam blocks. Simulations were completed with the foam blocks and different configurations of the rigid ISOFIX under the identical acceleration pulse for side impact for the Hybrid III 3-year-old dummy for all the three methods of CRS anchoring.

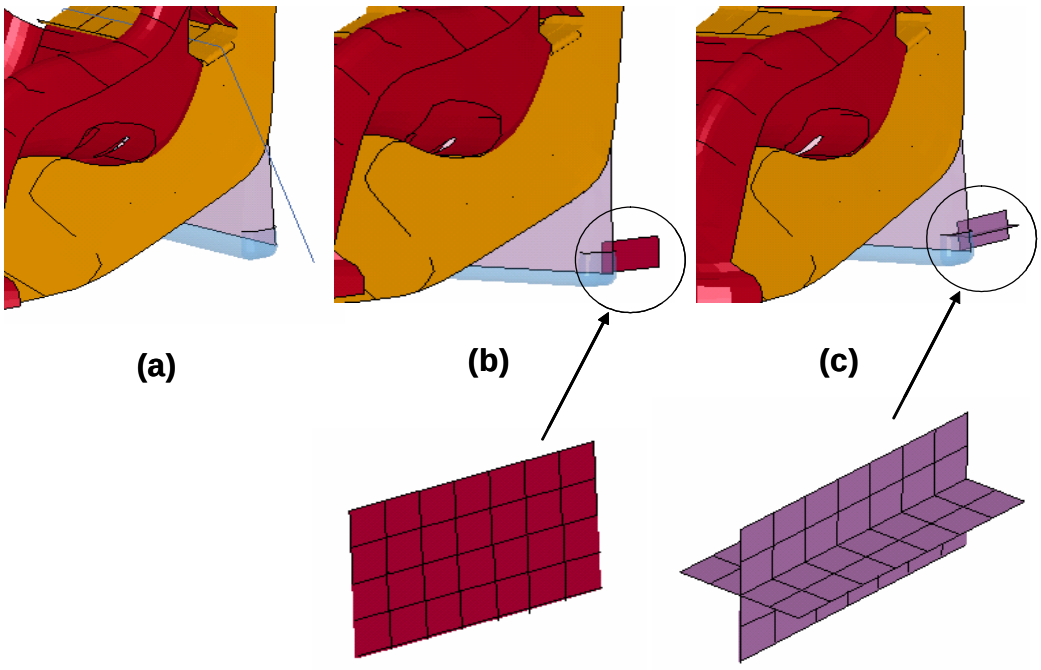

Figure 12. Different anchoring methods: (a) flexible LATCH, (b) rigid ISOFIX rectangular section, and (c) rigid ISOFIX cross-shaped section.

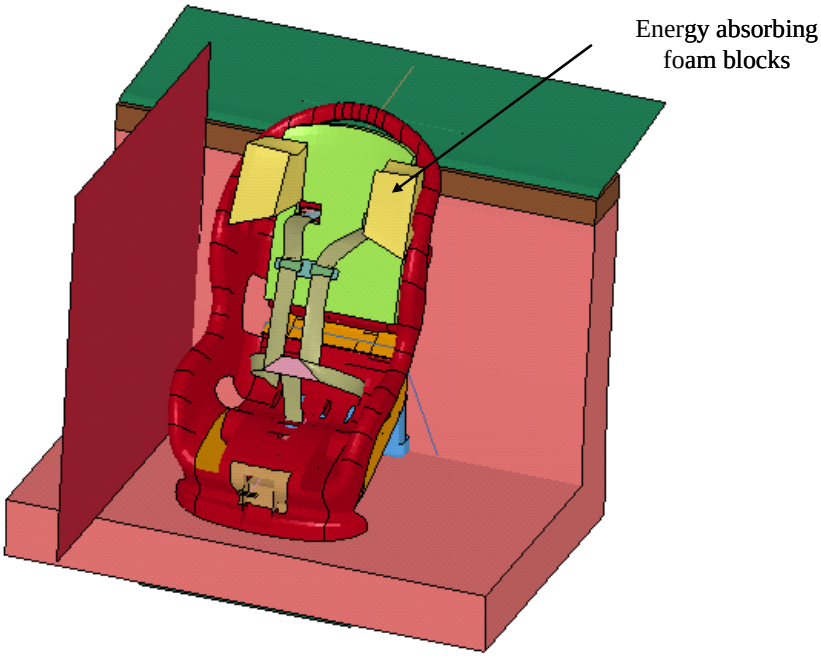

Figure 13. Finite element model of the CRS with additional energy absorbing foam blocks.

6.1 Qualitative Analysis

Figure 14 illustrates configuration for the Hybrid III 3-year-old at the times when maximum lateral displacement of the dummy and the CRS was observed. Flexible LATCH system exhibited the maximum lateral displacement of the CRS and the dummy. A CRS contact and foot contact occurred for the flexible LATCH anchoring. A reduction in lateral head and CRS displacement was observed for the rigid ISOFIX rectangular section, with minimal CRS contact. Use of the rigid ISOFIX system with cross-shaped section further reduced the lateral displacement of the head and the CRS. Contact between the CRS and the rigid wall was not observed for this configuration.

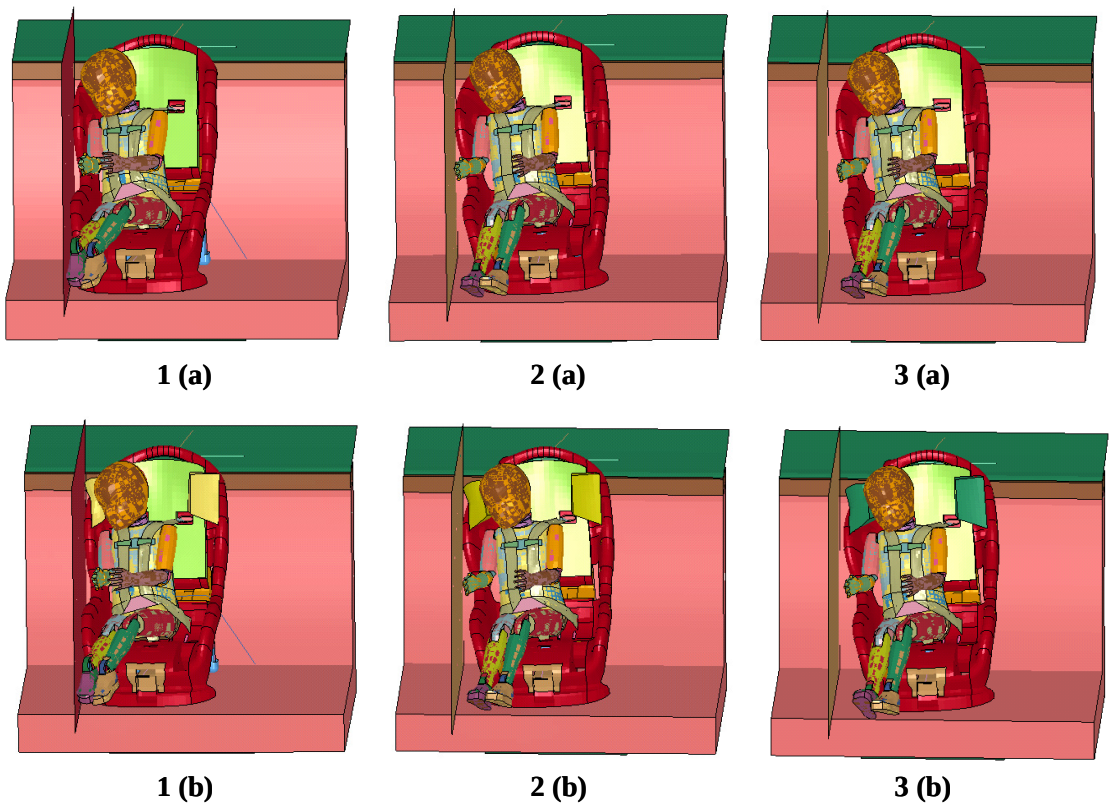

Figure 14. Maximum head and CRS displacement observed by the Hybrid III 3-year-old dummy for:

1. Flexible LATCH (a) without foam blocks, and (b) with foam blocks
2. Rigid ISOFIX rectangular section (a) without foam blocks, and (b) with foam blocks
3. Rigid ISOFIX cross-shaped section (a) without foam blocks, and (b) with foam blocks

6.2 Quantitative Analysis

6.2.1 Resultant Head Accelerations

Figure 15 illustrates the resultant head acceleration profiles as a function of time for all the three anchoring configurations (with and without foam) for the Hybrid III 3-year-old child dummy. Similar time profiles with similar peak values were observed for the resultant head acceleration for the Hybrid III 3-year-old child dummy for all the three anchoring configurations. Addition of foam was effective in reducing the head accelerations further by approximately 10 percent.

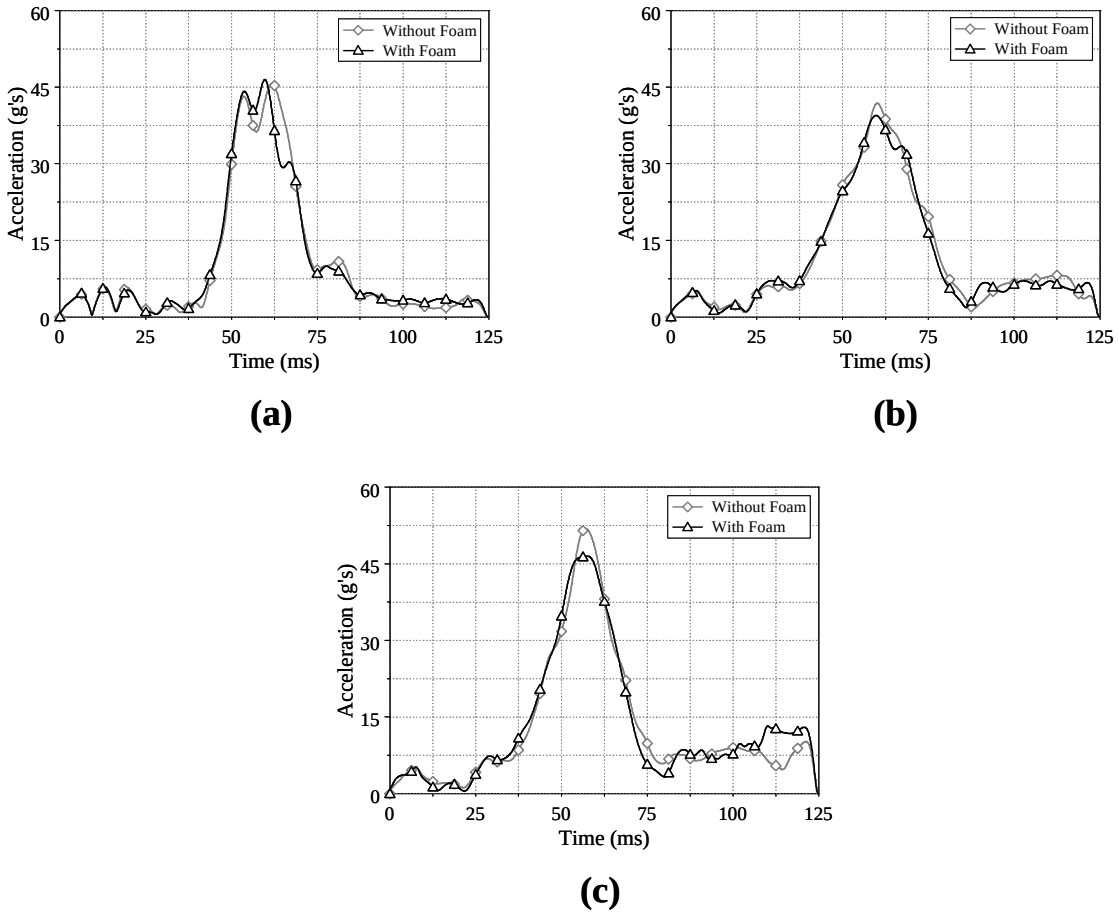

Figure 15. Resultant head acceleration profiles for the Hybrid III 3-year-old dummy as a function of time in the absence and presence of foam blocks for (a) flexible latch, (b) rigid ISOFIX rectangular section and (c) rigid ISOFIX cross-shaped section.

6.2.2 Resultant chest accelerations

The resultant chest acceleration time profiles are shown in Figures 16. It was observed that the rigid ISOFIX with the rectangular section was effective in reducing the resultant chest accelerations by approximately 50 percent for the Hybrid III 3-year-old dummy. Whereas the rigid ISOFIX system with cross-shaped section reduced the resultant chest accelerations by 40 percent compared to the values observed by the flexible LATCH configuration. Addition of energy absorbing foam further reduced the chest accelerations by approximately 5 percent for the child dummy.

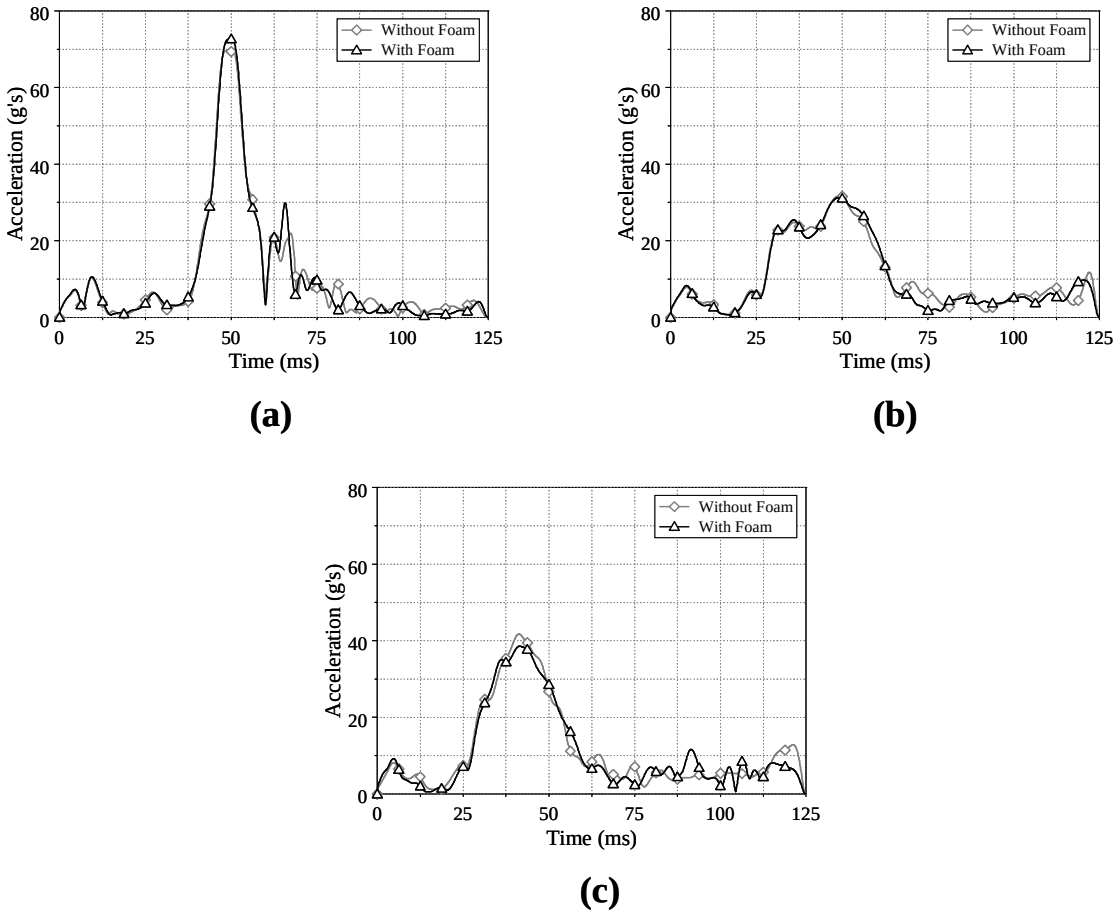

Figure 16. Resultant chest acceleration profiles for the Hybrid III 3-year-old dummy as a function of time in the absence and presence of foam blocks for (a) flexible latch, (b) rigid ISOFIX rectangular section and (c) rigid ISOFIX cross-shaped section.

6.2.3 Lateral shear

Figure 17 exhibits the lateral shear (F_Y) observed at the upper neck load cell for the Hybrid III child dummy as a function of time. A reduction of approximately 20 percent was observed for the Hybrid III child dummy by using rigid ISOFIX systems instead of the flexible LATCH. Addition of foam was effective in further reducing the lateral shear by approximately 20 percent.

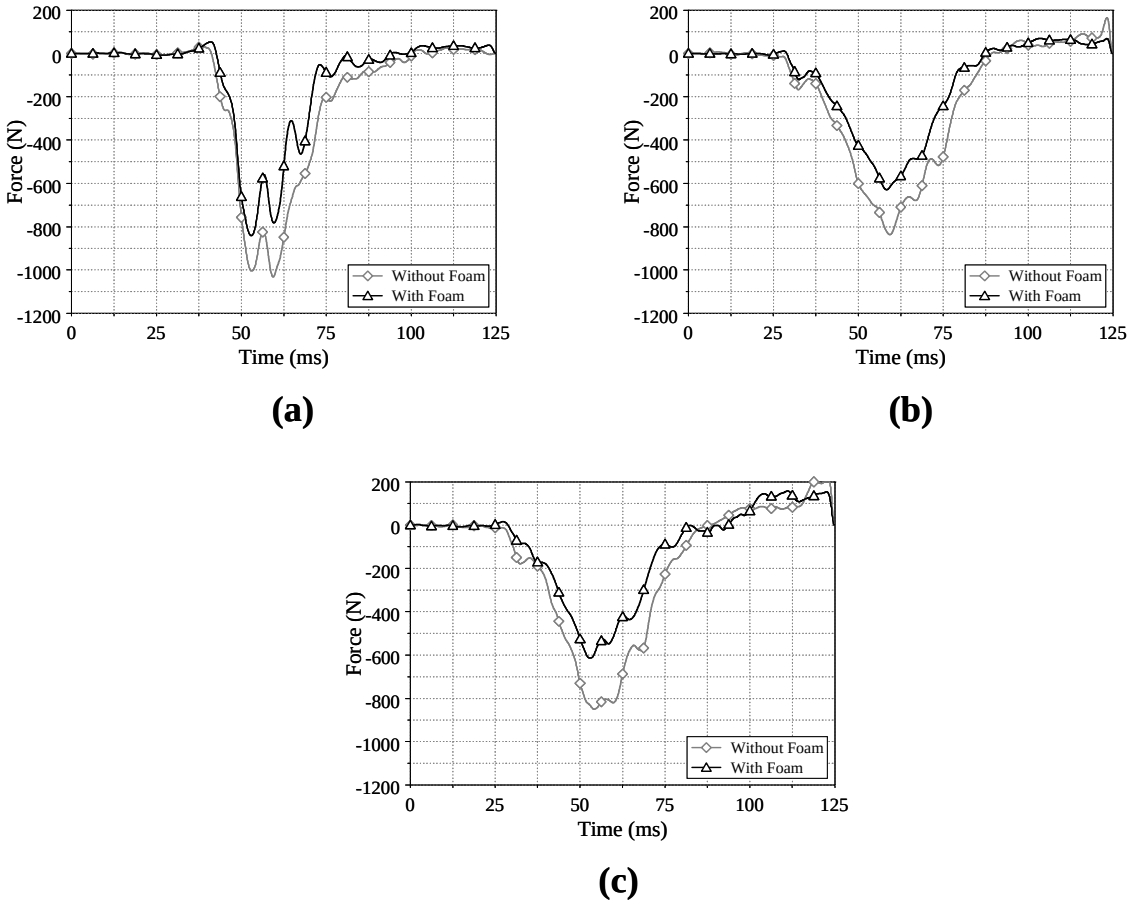

Figure 17. Lateral shear profiles for the Hybrid III child dummy as a function of time in the absence and presence of foam blocks for (a) flexible latch, (b) rigid ISOFIX rectangular section and (c) rigid ISOFIX cross-shaped section.

6.2.4 Lateral bending

Figure 18 illustrates the lateral bending (M_X) profiles as a function of time for all the three anchoring configurations (with and without foam) for the Hybrid III child dummy. The numerical Hybrid III dummy exhibited similar time profiles for the lateral bending with a difference in peak values. Use of rigid ISOFIX systems was observed to reduce the lateral bending by approximately 35 percent (rectangular section) and 30 percent (cross-shaped section) respectively. Addition of foam was observed to further reduce the lateral bending of the Hybrid III dummy's neck by 10 percent.

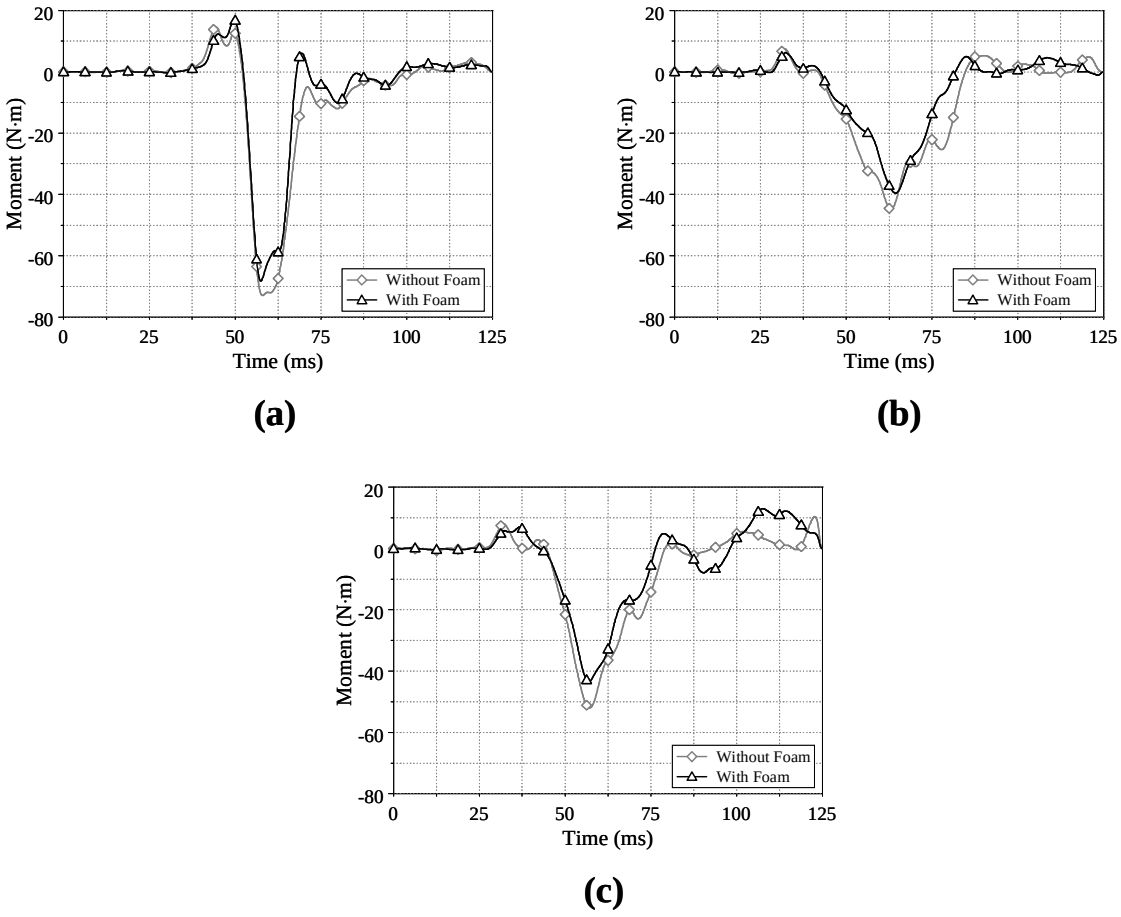

Figure 18. Lateral bending profiles for the Hybrid III child dummy as a function of time in the absence and presence of foam blocks for (a) flexible latch, (b) rigid ISOFIX rectangular section and (c) rigid ISOFIX cross-shaped section.

Tables 1 and 2 tabulate the peak values of different injury parameters including the lateral displacement of the center of gravity of the head for the Hybrid III child dummy. The lateral displacement of the head was reduced by 44 mm by using energy absorbing foam with rectangular section ISOFIX and 68 mm by using cross-shaped section ISOFIX respectively for the Hybrid III 3-year-old dummy compared to the flexible LATCH configuration.

Table 1. Peak values observed for the flexible LATCH, rigid ISOFIX (rectangular section) and rigid ISOFIX (cross-shaped section) configurations for the Hybrid III 3-year-old dummy.

	Flexible Latch	Rigid ISOFIX (Rectangular section)	Rigid ISOFIX (Cross-shaped section)
Head y-axis acceleration (g's)	-45.5	-39.5	-49.5
Chest y-axis acceleration (g's)	-68.2	-31.8	-41
Resultant head acceleration (g's)	45.7	41.6	51.8
Resultant chest acceleration (g's)	69	31.8	41.6
Head injury criteria (HIC-15)	161.2	117.6	180.8
Lateral Shear (N)	-1030	-836.6	-848.3
Lateral Bending (N.m)	-73	-44.8	-52
Lateral head cg displacement (mm)	253.6	224.2	202.2

Table 2. Peak values observed for the flexible LATCH, rigid ISOFIX (rectangular section) and rigid ISOFIX (cross-shaped section) configurations for the Hybrid III 3-year-old dummy in the presence of the energy absorbing foam.

	Flexible Latch	Rigid ISOFIX (Rectangular section)	Rigid ISOFIX (Cross-shaped section)
Head y-axis acceleration (g's)	-44.5	-37.5	-44
Chest y-axis acceleration (g's)	-71	-31	-38
Resultant head acceleration (g's)	46	38.9	46.4
Resultant chest acceleration (g's)	72.6	31.2	38.5
Head injury criteria (HIC-15)	157.4	109	171.5
Lateral Shear (N)	-832.2	-625.2	-612.4
Lateral Bending (N.m)	-69	-39.7	-43.5
Lateral head cg displacement (mm)	237.4	209.7	185.8

7. Conclusions

1. Side impact data comparisons for the Hybrid III 3-year-old child dummy were conducted between the simulation results with flexible LATCH and experimental findings obtained from NHTSA vehicle Crash Test Database [12]. Numerical simulations were observed to be in a good agreement with the experimental findings in terms of head and chest local *y*-axis accelerations, and upper and lower neck forces. The resultant upper and lower neck moments of the child dummy were over predicted by the numerical model.

2. Use of rigid ISOFIX systems effectively reduced the chest accelerations by 50 percent (rectangular section) and 40 percent (cross-shaped) section for the Hybrid III 3-year-old child dummy. A reduction of approximately 20 percent was observed in the lateral shear and 30 to 35 percent in the lateral bending for the Hybrid III child dummy by using rigid ISOFIX systems instead of the flexible LATCH.

3. Addition of energy absorbing foam blocks was effective in further reducing the injury parameters and the lateral displacement of the dummy's head. The lateral displacement of the head was reduced by 44 mm by using energy absorbing foam blocks with rectangular section ISOFIX and 68 mm by using cross-shaped section ISOFIX respectively for the Hybrid III 3-year-old dummy compared to the flexible LATCH configuration. In near-side impact situations the main cause of injury is contact related [5, 6]. A cross-shaped rigid ISOFIX system in the presence of energy absorbing foam blocks has shown a capability of reducing the amount of injury incurred during a near-side impact.

8. Acknowledgements

Financial support provided by the Auto21 Network Centres of Excellence is gratefully acknowledged.

References

1. National Highway Traffic Safety Administration (2005). Traffic Safety Facts 2005 (DOT HS 810 618 pp. 1-6). U.S. Department of Transportation.

2. Statistics Canada (2003). Major Causes of Death, Government of Canada. <http://142.206.72.67/02/02b/02b_003_e.htm> Accessed February 2007.

3. Final rule (2003). Federal Motor Vehicle Safety Standards 213: Child Restraint Systems. 49 CFR Part 571, Docket No. NHTSA–03–15351, Federal Register, Vol. 68, No. 121, pp. 1-40.

4. Advance notice of proposed rulemaking (2002). Federal Motor Vehicle Safety Standards 213: Child Restraint Systems. 49 CFR Part 571, Docket No. 02–12151, Federal Register, Vol. 67, No. 84, pp. 1-17.

5. Howard A, Rothman L, Moses A, Pazmino-Canizares J, Monk B, Comeau J, Mills D, Beng S, Hale I and German A (2004). Children in Side-Impact Motor Vehicle Crashes: Seating Positions and Injury Mechanisms. The Journal of TRAUMA Injury, Infection, and Critical Care, Vol. 56, pp. 1276 –1285.

6. Newgard CD, Lewis RJ, Kraus JF and McConnell KJ (2005) Seat position and the risk of serious thoracoabdominal injury in lateral motor vehicle crashes. Accident Analysis and Prevention, Vol. 37, pp. 668-674.

7. Transport Canada (2002). Motor Vehicle Safety Acts. Government of Canada. <http://www.tc.gc.ca/acts-regulations/mvsa/regulations/mvsrg/210/mvs210.html> Accessed November 2007.

8. United Nations Economic Commission for Europe (2006). Uniform provisions concerning the approval of vehicles with regard to safety-belt anchorages, ISOFIX anchorage systems and ISOFIX top tether anchorages. Rev.1/Add.13/Rev.4. pp. 1-74. < http://www.unece.org/trans/main/wp29/wp29regs/r014r4e.pdf> Accessed December 2007.

9. Charlton J, Fildes B, Laemmle R, Smith S and Douglas F (2004). A Preliminary Evaluation of Child Restraint Crash Performance with Three Anchorage Systems in a Holden Commodore. Australasian Road Safety Research, Policing and Education Conference Proceedings, pp. 1-10. <http://www.rsconference.com/pdf/RS040079.pdf> Accessed January 2007.

10. CLEPA (2004). Side Impact and Ease of Use Comparison between ISOFIX and LATCH. Presentation to GRSP, Informal Document GRSP-35 -1 9, Geneva, May 2004, pp. 1-31 <http://www.unece.org/trans/doc/2004/wp29grsp/TRANS-WP29-GRSP-35-inf19e.pdf> Accessed January 2007.

11. Klinich K, Ritchie N, Manary M, Reed M, Tambora N and Schneider L (2005). Kinematics of the Q3s ATD in a child restraint in a far side impact loading. 19th Enhanced Safety of vehicles Conference, Paper No 05-0262, June 6-9, 2005, Washington D.C.

12. NHTSA Vehicle Crash Test Database. Test no. 4585. < http://www-nrd.nhtsa.dot.gov/database/aspx/vehdb/querytesttable.aspx> Accessed August 2007.

13. SAE J211/1 Instrumentation for Impact Test - Part 1– Electronic Instrumentation. (2003). Society of Automotive Engineers, Warrendale, PA.

14. American Standard of Testing Methods. (2004). Standard test methods for tensile properties of plastics [Metric]. (Designation: D638M). Annual book of ASTM standards, Philadelphia, PA, USA.

15. Turchi R, Altenhof W, Kapoor T, Howard A, (2004). An investigation into the head and neck injury potential of three-year-old children in forward and rearward facing child safety seats. International Journal of Crashworthiness, Vol. 9 (4), pp. 419-431.

16. LS-DYNA model of the Hybrid III 3 year old child dummy - version 2.3B2. (2000). Users Manual, First Technology Safety Systems, Plymouth, MI.

17. Hallquist. JO, (1998). LS-DYNA theoretical manual, Livermore Software Technology Corporation, Livermore CA.

18. Wang Q, Kapoor T, Altenhof W, Howard A, (2006). A Numerical Investigation into the injury potential of three-year-old children seated in forward facing child safety seats during side impact crashes in far side configurations. 9th International LS-DYNA Users Conference.